Intervalence Charge Transfer in Aluminum Oxide and Aluminosilicate Minerals at Elevated Temperatures

(running title: Intervalence Charge Transfer at High Temperatures)

9088 words

Helen V. Evans, †George R. Rossman

hvevans@caltech.edu; grr@caltech.edu

†Corresponding author

Division of Geological and Planetary Sciences, California Institute of Technology, Pasadena, California 91125-2500, U.S.A.

ABSTRACT

Single-crystal optical spectra of corundum (Al_2O_3) and the Al_2SiO_5 polymorphs andalusite, kyanite, and sillimanite, containing both $Fe^{2+} – Fe^{3+}$ and $Fe^{2+} – Ti^{4+}$ intervalence charge transfer (IVCT) absorption bands were measured at temperatures up to 1000 °C. Upon heating, thermally equilibrated IVCT bands significantly decreased in intensity and recovered fully on cooling. These trends contrast with the behavior of crystal field bands at temperature for Fe, Cr and V in corundum, kyanite, and spinel. The effects of cation diffusion and aggregation, as well as the redistribution of band intensity at temperature, are also discussed. The loss of absorption intensity in the visible and near-infrared regions of the spectrum of these phases may point to a more general behavior of IVCT in minerals at temperatures within the Earth with implications for radiative conductivity within the Earth.

Keywords: intervalence charge transfer, temperature dependence, corundum, andalusite, kyanite, sillimanite

INTRODUCTION

In intervalence charge transfer (IVCT), an electron "hops" transiently from a donor to an acceptor metal cation due to an optical or a thermal excitation (Sherman 1987a,b). This process dominates the coloration of many minerals (Fritsch and Rossman 1988) and has numerous materials applications such as luminescence, semiconductors, and catalysis (Blasse 1991; Hammarström 2015). Terminology surrounding charge transfer phenomena varies widely depending on discipline and theoretical framework. Though other models like small polaron hopping are also used for this kind of process (Hush 1968), the term "IVCT" more specifically originates from Hush theory first described by Allen and Hush (1967) and Hush (1967). It is an umbrella term encompassing a broad range of optical transitions involving charge transfer where electrons are "nearly" localized to the fields of participating metal cations. In the solid state, "nearly localized sites" usually indicates adjacent cation sites; longer range electron transfer is unlikely except in systems with more polymerized structures like chains and sheets (Amthauer and Rossman 1984). The "IVCT" designation typically excludes the weak interaction limit where cation pairs are at most exchange-coupled; the associated *d-d* electronic transitions would instead be analyzed through ligand field theory.

Electron delocalization is facilitated via orbital overlap, of which two forms are important: direct overlap between metal cations; and metal-ligand-metal overlap bridged through weak metal-ligand bonding (Hush 1967). The character of IVCT in a particular system depends both on the overall degree of delocalization across cation sites and the individual values of the

integrals for direct and ligand-bridged orbital overlap between metal cations. Thus, it varies significantly depending on the constituent metals and ligands as well as the local geometry. When known, the details of the orbital overlap between two metal cations that engage in IVCT are specified, typically through theoretical work such as TD-DFT calculations (*e.g.* Hunault et al 2017). Most frequently, however, the label "IVCT" is applied to visible region features in absorption spectra where it is assumed – based both on general accumulated lore about IVCT transitions and on what is known about a specific system – that ligand-bridged overlap across shared edges or faces of cation polyhedra dominates for that transition (*e.g.* Moon and Phillips 1994).

Broad absorption bands polarized in the direction of the metal-metal bond are typically diagnostic of IVCT in single crystal optical spectra. The full-width at half-height (FWHM) range 3000-4000 cm^{-1} tends to be used loosely as a lower cutoff, while 4000-5000 cm^{-1} and above can be assigned with greater confidence to IVCT (Mattson and Rossman 1987a,b, 1988). Nonetheless, there is some nuance involved in appropriately assigning a band to IVCT. For instance, narrower IVCT bands have similar diagnostic properties to intensified crystal field bands (Mattson and Rossman 1987a, b; Smith 1978; Taran et al. 1996). A particularly broad absorption feature may also be more appropriately expressed under some circumstances as the sum of two or more components rather than a band for a single IVCT transition (Geiger and Taran 2023).

IVCT in minerals can be a feature of the phase's stoichiometry but more commonly occurs between metal cations substituting into the structure at low concentrations. Typically, cations are oxo-bridged and adopt octahedral-octahedral site geometries (Burns 1993), though other configurations have been observed such as octahedral-dodecahedral in garnet (Taran et al. 2007).

This is the peer-reviewed, final accepted version for American Mineralogist, published by the Mineralogical Society of America.
The published version is subject to change. Cite as Authors (Year) Title. American Mineralogist, in press.
DOI: https://doi.org/10.2138/am-2024-9343. http://www.minsocam.org/

An additional soft diagnostic in minerals is band intensity: due to the selection rules for crystal field transitions in distorted octahedral sites, single cation *d-d* bands tend to be less intense than IVCT bands, even at relatively low IVCT pair concentrations. Intensities of spin-allowed IVCT transitions have been found to be one to three orders of magnitude higher than spin-allowed *d-d* transitions (Smith and Strens 1976). Cation species that participate in IVCT are also limited in natural terrestrial minerals: all commonly occurring cases to date involve iron. The homonuclear symmetric electron transfer $Fe^{2+} + Fe^{3+} \rightarrow Fe^{3+} + Fe^{2+}$ and heteronuclear asymmetric electron transfer $Fe^{2+} + Ti^{4+} \rightarrow Fe^{3+} + Ti^{3+}$ processes are both commonly observed in many mineral spectra (Rossman 2024).

In corundum (α-Al_2O_3), iron and titanium substituting for aluminum can produce both Fe/Ti and Fe/Fe IVCT couples. These along with ferric iron – both as single Fe^{3+} cations and as exchange-coupled Fe^{3+}/Fe^{3+} pairs – are the primary cation species that contribute to the optical spectrum of Fe,Ti-containing corundum (Dubinsky et al. 2020). General opinion concurs with early work (Ferguson and Fielding 1971, 1972) assigning the 580 and 700 nm features to Fe/Ti IVCT in edge- and face-sharing geometries, respectively. Correspondingly, features near 880 and 1110 nm are typically assigned to edge- and face-sharing Fe/Fe IVCT, respectively (Moon and Phillips 1994).

No consensus has yet been reached on the precise nature of the Fe/Ti defects in corundum. Experimental work has indicated that iron and titanium may form more complex clusters in corundum, perhaps involving additional cations and/or vacancies (Moon and Phillips 1994). It is also possible that, as similar Fe/Ti IVCT bands in some organometallic molecular species have been found to be, corundum's IVCT bands are more metal-centered, "contaminated" with *d-d* character in the excited state (Turlington et al. 2016; Livshits et al. 2019). While TD-DFT studies

This is the peer-reviewed, final accepted version for American Mineralogist, published by the Mineralogical Society of America.
The published version is subject to change. Cite as Authors (Year) Title. American Mineralogist, in press.
DOI: https://doi.org/10.2138/am-2024-9343. http://www.minsocam.org/

have confirmed that three cation clusters are a possibility (Bristow et al. 2014), the extent to which Fe/Ti IVCT in corundum may be subject to additional short-range ordering is not known.

Optical absorption spectroscopy at moderately elevated temperatures has been used to characterize *d-d* components in crystal field band systems (Taran et al. 1994, 2005; Taran and Langer 2001; Ullrich et al. 2002, 2004). Fewer studies have applied this technique to IVCT systems, as the effect of temperature on IVCT bands has been considered in the past to be relatively minor (Burns 1993). Some isolated studies of specific systems such as biotite at elevated temperatures (Rüscher 2012) exist, but Taran and Langer (1998) have done the most extensive work to date on the high temperature behavior of Fe/Ti and Fe/Fe IVCT bands across a variety of mineral species. They examined the optical and near-infrared absorption spectra of several major rock-forming minerals containing Fe^{2+} - Fe^{3+} or Fe^{2+} - Ti^{4+} pairs at temperatures from 300 to 900 K. The integral intensity was found to generally decrease and the energy to shift slightly towards lower values, with a more pronounced decrease in intensity for Fe^{2+} - Fe^{3+} than for Fe^{2+} - Ti^{4+} pairs; all changes were found to be reversible.

These authors explain the decrease in IVCT band intensity with rising temperature as being due to increased electron delocalization along the M–M bond from thermal vibrations. The more symmetric the IVCT transition, the smaller the activation energy for electron transfer; the smaller the activation energy for electron transfer, the stronger the inverse dependence of band intensity on temperature observed for a particular mineral. Generally, the primary factors affecting activation energy would be inherent energetic differences between the sites or metal ions involved – ex: Fe/Fe IVCT being more symmetric than Fe/Ti – and the level of coupling between sites due to the M–M bond length. Rüscher (2012) adds that below $T_D/2$ (T_D = Debye temperature), a temperature-independent "disorder energy" term will dominate the overall

activation energy for polaron hopping, leading to a decrease in the activation energy at lower temperatures. Small polarons in disordered systems likely experience a "pinning effect" that causes the higher observed absorption band intensities at lower temperatures.

It is notable that among the minerals studied by Taran and Langer (1998), the Fe/Fe and Fe/Ti IVCT bands examined showing the strongest decrease in integral intensity at elevated temperature were both in corundum. It is also of interest that the Fe/Ti IVCT bands in corundum are much lower in energy than those observed in stoichiometric Fe/Ti minerals (Mattson and Rossman 1988). Only two other well-documented minerals have bands with similar parameters that have been ascribed by most authors to Fe/Ti IVCT: the Al_2SiO_5 polymorphs kyanite (Smith and Strens 1976; Parkin et al. 1977; Platonov et al. 1998) and sillimanite (Rossman et al. 1982). Closer examination at higher temperatures of the IVCT bands in corundum and similar minerals with unusual Fe/Ti band assignments may, then, be of some fundamental interest.

Extending the measurement range of IVCT minerals is also important for understanding conditions in the deep earth due to the abundance of iron at depth. The behavior of IVCT absorption bands at these temperatures has potential geophysical implications related to calculations for radiative heat transport in the mantle (Hofmeister 2005; Keppler et al. 2008; Keppler and Smyth 2005; Lin et al. 2013; Gross and Afonso 2019). The thermal behavior of corundum's Fe/Ti bands may give insight into the behavior of Fe/Ti bands in upper mantle phases such as ilmenite ($FeTiO_3$), a superstructure of corundum, which would also be of interest as a stoichiometric IVCT mineral. Though characterizing ilmenite via absorption spectroscopy is challenging due to its high opacity, investigating the dilute case in corundum could provide illumination: recent unpolarized spectra of ilmenite reveal what appears to be similar band

This is the peer-reviewed, final accepted version for American Mineralogist, published by the Mineralogical Society of America.
The published version is subject to change. Cite as Authors (Year) Title. American Mineralogist, in press.
DOI: https://doi.org/10.2138/am-2024-9343. http://www.minsocam.org/

136 structure to corundum's Fe/Ti IVCT bands, red-shifted to near-infrared wavelengths (Taran
137 2019).

138

139 # EXPERIMENTAL DETAILS

140 ## Sample preparation

141 Minerals (Table 1) were oriented for polarized optical and FTIR spectroscopy by examination
142 of cleavage, pleochroism and interference figures as well as spindle stage methods, and made
143 into polished thin slabs. Further information on the samples used, including type locality and any
144 visual changes that were observed with heating, is provided in the Supplemental Documentation.
145 All corundum samples were prepared in the E⊥c orientation, while the aluminosilicate samples
146 all had more than one orientation available. The measured orientations of all spectra are specified
147 in the relevant figure descriptions. Sample thicknesses varied from 0.302 to 4.12 mm. All data
148 presented in the figures have been normalized to 1.00 mm thickness except for sillimanite, which
149 is displayed at 4.00 mm thickness.

150 ## Analytical methods

151 Elemental analyses (Table 2) were conducted with an INAM EXPERT 3L X-ray fluorescence
152 unit. The Fe and Cr contents obtained from these scans are the most reliable. Scans were run
153 without a helium atmosphere, adding uncertainty to the light elements analysis. The machine
154 uses a titanium target, adding uncertainty to any low-level measurement of Ti content.

155 Spectra were obtained in a Linkam TS-1500 heating stage, which was refitted with a thicker
156 (1.34 mm) glass lower window to reduce the effect of interference fringes. Samples were placed

in a ceramic crucible within the stage chamber; light passes through a 1.7 mm diameter hole in the base of the crucible.

Optical spectra were taken with a home-built 1024 element silicon diode-array spectrometer with a fixed orientation calcite polarizer. Fifty-one transmission mode scans were collected and averaged for each measurement. Data were acquired over two wavelength ranges: 380 nm to 1100 nm (visible mode) and 930 to 1700 nm (NIR mode). Utilizing both ranges required switching detectors, which in turn required heating a sample twice—once in each mode. Extended range near-infrared spectra for the Fe^{2+} spinel were taken on a ThermoNicolet iS50 FTIR spectrometer in transmission mode at 4 cm^{-1} resolution using a silica beamsplitter, a tungsten-halogen white light source, and an MCT-A detector, interfaced with a Continuμm IR microscope with a 10× glass objective.

Visible and NIR spectra from the diode-array spectrometer for any given temperature were merged in absorbance: one spectrum was offset vertically so both spectra overlapped across a common range. Data from the diode-array and the FTIR spectrometers were merged in transmittance: a linear transform was applied to the FTIR data to correct numerically for both attenuation and blackbody radiation. The constant offset and linear transform were optimized via least-squares regression analysis.

Merging spectra from two separate runs assumes that no significant changes occurred in the samples between the two heating cycles. Consequently, only the visible mode of the diode-array spectrometer was used for most of the *d-d* systems, where features of interest were not expected to extend into the NIR. The breadth of IVCT bands, however, incentivized the use of data from both modes where possible.

This is the peer-reviewed, final accepted version for American Mineralogist, published by the Mineralogical Society of America.
The published version is subject to change. Cite as Authors (Year) Title. American Mineralogist, in press.
DOI: https://doi.org/10.2138/am-2024-9343. http://www.minsocam.org/

Care was taken to maintain the same spot between measurements, as many of the IVCT samples were zoned. Because andalusite, kyanite and sillimanite have distinct extinction directions, a rotation adjustment of the furnace stage containing the sample was required before data collection; both a starting and an ending background was recorded for these samples, and only visible region data were used. For corundum samples, which were prepared in a single orientation, the furnace stage remained locked in place. After initial calibration to determine appropriate exposure times in both modes, samples could be sealed within the furnace to have visible and NIR spectra taken in succession. Visible spectra obtained a background measurement at the start of the experiment; NIR spectra obtained the background measurement at the end.

Before each heating run, the sample chamber was purged for at least 15 minutes with inert gas at a flow rate of ~150 ml/min which was sustained throughout the run. The type of inert gas used was optimized based on market forces of supply and demand: N_2 gas was used for all *d*-*d* band system samples; Ar gas was used for all IVCT samples. The heating stage itself was cooled with flowing ice water, which helped minimize baseline drift during heating. Samples were rapidly heated and cooled at a rate of 100 °C per minute. Spectra were taken at 100 °C intervals from 100 to 1000 °C, as well as room temperature at the start and end of the experiment. Final spectra were taken after a two-minute delay, which allowed the sample to reach thermal equilibrium.

Empirical correction for blackbody radiation

On the diode-array spectrometer, two measurements were taken after the two-minute delay: one with and one without source radiation blocked. The former allowed for correction for blackbody radiation coming from the sample. Data without source radiation were taken at all temperatures including room temperature and subtracted as transmittance from the normal data

This is the peer-reviewed, final accepted version for American Mineralogist, published by the Mineralogical Society of America.
The published version is subject to change. Cite as Authors (Year) Title. American Mineralogist, in press.
DOI: https://doi.org/10.2138/am-2024-9343. http://www.minsocam.org/

with an unblocked light source. No blackbody contribution was expected at room temperature, but subtracting "no source" from all data ensured that any systematic error within the empirical correction (a baseline shift) would be applied consistently to all data. Due to signal falloff, the "no source" data was cut off at short visible range wavelengths. At and below the cutoff, the correction was set to a constant in transmittance. The cutoff wavelength for each sample was determined empirically based on the location of a point of inflection in the no source data; the same cutoff was then applied to all temperatures for that sample, during that particular temperature run.

Numerical methods

While experimental precautions to ensure a relatively consistent coolant temperature helped minimize baseline drift, it was found that even small amounts of drift could be significant at temperatures near 1000 °C. Least-squares regression analysis was used to optimize the relative alignment of blackbody corrected data with nearest-temperature pairs (*e.g.* 1000 °C-heat versus 900 °C-cool, 900 °C-cool versus 800 °C-cool, and so on). The spectral regions chosen for alignment in most cases were either those that represented zero absorbance or that were expected to show little change between steps in temperature. When no such region could be found between a spectrum at temperature and its nearest-temperature pair, that spectrum was compared against spectra at other temperatures, both from that heating run and from any other heating runs done for that sample, as well as room temperature calibration data before any heating was done. This process was most straightforward for datasets with merged visible and NIR data. Only for first heating runs of predominantly Fe/Fe IVCT corundum samples (Supplemental Data) were no attempts made to correct for drift, as deconvolution of its effects from everything else going on proved to be difficult.

This is the peer-reviewed, final accepted version for American Mineralogist, published by the Mineralogical Society of America.
The published version is subject to change. Cite as Authors (Year) Title. American Mineralogist, in press.
DOI: https://doi.org/10.2138/am-2024-9343. http://www.minsocam.org/

Approximate curve fitting was done with a homemade Python script using the NumPy, SciPy and Matplotlib packages. Absorption spectra converted to wavenumber were successively fit as a sum of Gaussian and Lorentzian components. Fit quality was judged using studentized residuals; to reduce the likelihood of over-fitting, the "best" fits were chosen to minimize the number of components used. In many cases, there is some ambiguity in how to model the background of spectra at higher temperatures, particularly when the UV absorption edge contributes strongly to the spectrum. There may be some uncertainty in such fits; where fits have been included, it is largely to facilitate understanding beyond simple inspection of what shifts are occurring at elevated temperatures.

RESULTS

Note on abbreviations

Throughout this section, the label "STP" (standard temperature and pressure) will be used as needed to specify that a band under discussion is being referred to using its center at room temperature.

Corundum

An initial observation was that when a blue sapphire is heated to temperatures near or above the geological formation temperature, its color is lost; when it is cooled, the color returns (Supplemental Figure 1). Sapphire's blue color originates from Fe^{3+} *d*-*d*, Fe/Ti IVCT and Fe/Fe IVCT features that occur in the absorption spectra of natural corundum samples. To better understand how elevated temperature conditions perturb the IVCT bands, samples were tested that separate these features. Three corundum samples are discussed in the main text: one Fe^{3+}

This is the peer-reviewed, final accepted version for American Mineralogist, published by the Mineralogical Society of America.
The published version is subject to change. Cite as Authors (Year) Title. American Mineralogist, in press.
DOI: https://doi.org/10.2138/am-2024-9343. http://www.minsocam.org/

dominant (Figure 1), one Fe/Ti IVCT dominant (Figure 2), and one Fe/Fe IVCT dominant (Figure 3). Corroborating spectra with additional samples are provided in the Supplemental Data.

Fe^{3+} corundum. The bands centered at room temperature around 558, 717, and 915 nm (Supplemental Table 2) are best assigned to IVCT transitions. The most significant change observed to these bands is the decrease in their intensities: the edge-sharing Fe/Ti, face-sharing Fe/Ti, and edge-sharing Fe/Fe IVCT bands decrease by 65, 87 and 43 percent, respectively, in integral absorbance from room temperature to 1000 °C. In the recovery spectrum, the Fe/Ti IVCT bands decrease slightly in integral intensity – edge-sharing by 10 percent and face-sharing by 8 percent – while the edge-sharing Fe/Fe IVCT band increases by 34 percent. Some cation diffusion occurs during heating, causing the differences in relative band intensities between the starting and ending room temperature spectra.

Fe/Ti corundum. After the initial heating of a corundum sample where the 580 and 700 nm Fe/Ti features dominate the visible spectrum (Supplemental Figures 2a,b), the recovery spectrum is noticeably different: some rearrangement of band intensity occurs within the Fe/Ti IVCT region, and absorption increases at short and long wavelengths.

Its second heating is given in Figure 2. At room temperature, a band at 575 nm is the primary fitted Gaussian component (Supplemental Table 3) that is compatible with an IVCT assignment; its parameters line up well with reported values for the edge-sharing Fe/Ti IVCT band (Moon and Phillips 1994). The 707 nm band has a half-width more akin to that of a *d-d* band (Mattson and Rossman 1988) but is of an appropriate energy for face-sharing Fe/Ti IVCT. There are two corresponding long wavelength features: the 819 nm band, which has a borderline half-width for IVCT; and the 1056 nm band, which has a half-width that better suits a *d-d* assignment. These

likely correspond to features that have previously been assigned to Fe/Fe IVCT elsewhere, only with minor differences in their local environment.

At higher temperatures, an additional broad Gaussian component is required near 500 nm: 515 nm at 500 °C and 483 nm at 1000 °C. The numerical values for these fits may be somewhat questionable at short wavelengths due to red shifting of the UV absorption edge and the breadth of absorbance in the region in question.

At 1000 °C, the Fe/Ti bands altogether lose 74 percent of their integral intensity at 1000 °C relative to room temperature. Individually, the 575 nm (STP) band decreases by 73 percent and the 707 nm (STP) band by 79 percent. Over the course of heating, the Fe/Ti bands are radically diminished relative to the Fe/Fe bands. Combined, the Fe/Fe bands lose 33 percent of their integral intensity, the 819 nm (STP) band decreasing by 31 percent and the 1056 nm (STP) band by 47 percent. This deviates from the expectation for simple isolated Fe/Ti versus Fe/Fe pair bands as asymmetric and symmetric IVCT processes, respectively. It is also observed that the 575 nm Fe/Ti band strongly red shifts, while the center of the 707 nm Fe/Ti band stays at nearly the same energy.

Fe/Fe corundum. The recovery spectrum of a corundum sample with relatively high iron content and a dominating ~880 nm feature after an initial heating experiment (Supplemental Figures 4-GS) is also altered substantially: the 580 nm Fe/Ti feature diminishes, while the 880 nm feature grows asymmetrically at longer wavelengths. This has been found to occur both in samples with convincingly measurable titanium content (Supplemental Figures 4-BS) and in samples with minimal amounts of titanium (Supplemental Table 4a), below the detection limit of our machine.

Changes in recovery after the second heating run (Figure 3) are negligible. At room temperature, the wavelength region that contains the Fe/Ti and Fe/Fe IVCT bands can be fit (Supplemental Tables 4c, 4d) using three broad Gaussian components: 548 nm, 748 nm, and 907 nm. As in previous corundum samples, these bands correspond to features widely assigned to edge-sharing Fe/Ti, face-sharing Fe/Ti, and edge-sharing Fe/Fe IVCT, respectively. While the calculated band centers deviate somewhat from standard literature values, that is likely attributable primarily to slight differences in local environment; similar band parameters have been found in other natural Australian corundum samples (Taran and Langer 1998). All three bands strongly decrease in intensity at temperature.

During heating, significant changes in the configuration of these bands occur. At 500 °C, the 548 nm and 748 nm Fe/Ti bands red shift and blue shift, respectively, both centers moving towards previously reported literature values. The 907 nm Fe/Fe band is split into two components: 834 nm and 980 nm.

At 1000 °C, only one Gaussian component is required to represent the Fe/Ti bands: 617 nm. To adopt this configuration, the 548 nm edge-sharing and 748 nm face-sharing Fe/Ti bands would need to be strongly red-shifted or blue-shifted, respectively, relative to room temperature.

This is the peer-reviewed, final accepted version for American Mineralogist, published by the Mineralogical Society of America.
The published version is subject to change. Cite as Authors (Year) Title. American Mineralogist, in press.
DOI: https://doi.org/10.2138/am-2024-9343. http://www.minsocam.org/

It is plausible, given the thermal trends observed at 500 °C, that these shifts both occur and that both Fe/Ti bands converge to the 617 nm component at 1000 °C. Overall, this would represent a 65 percent decrease in integral intensity. If it is instead assumed that only the edge-sharing band contributes to the 617 nm band, then the 548 nm (STP) band decreases 42 percent in integral intensity and the 748 nm band fully depletes by 1000 °C, which is still a significant reduction in absorbance attributable to Fe/Ti IVCT.

As expected for symmetric charge transfer, the intensity of the Fe/Fe pair band decreases more strongly than that of the Fe/Ti IVCT bands: the combined integral intensity of the 813 and 1018 nm components at 1000 °C represents a 74 percent decrease from the 907 nm band intensity at room temperature.

Al_2SiO_5 polymorphs

One of each Al_2SiO_5 polymorph is discussed: a low-Cr IVCT kyanite (Figure 4), a sillimanite (Figure 5), and an andalusite. Two heating experiments were conducted on the andalusite: Figure 6 provides variable temperature spectra for the first and Figure 7 for the second experiment.

IVCT kyanite. Three Gaussian components (Supplemental Table 5a) are broad enough to be assigned to IVCT. The 611 and 821 nm bands correspond to features near 625 nm and 833 nm others have assigned (Platonov et al. 1998) to Fe/Ti and Fe/Fe IVCT, respectively.

During early heating, these two bands show limited change in integral intensity; the fitted components also blue shift and broaden slightly. Meanwhile, the short wavelength region (<~550 nm) becomes substantially more absorbing. After 500 °C, the short wavelength region no longer broadly increases, and the Fe/Ti and Fe/Fe IVCT bands rapidly lose intensity. From 500 to 1000

This is the peer-reviewed, final accepted version for American Mineralogist, published by the Mineralogical Society of America.
The published version is subject to change. Cite as Authors (Year) Title. American Mineralogist, in press.
DOI: https://doi.org/10.2138/am-2024-9343. http://www.minsocam.org/

°C, they decrease by 36 and 69 percent, respectively – for comparison, 34 and 69 percent, respectively, from room temperature.

On cooling, these two bands fully recover their intensities. The short wavelength feature is found to broaden and increase in integral intensity, but these differences are relatively minor: most of the change that was observed at temperature in kyanite does not persist in the recovery spectrum.

Sillimanite. The room temperature spectrum reveals a complex band system. Its thermal trends are not obvious via inspection; several features (Supplemental Table 6c), likely related to crystal field transitions, are superimposed over the IVCT bands (Supplemental Table 6a).

The ~600 nm feature represents the sum of two components: a broad band at 592 nm and a narrower one at 617 nm. The 592 nm band has been assigned previously to Fe/Ti IVCT (Rossman et al. 1982) who also suggested that the 617 nm feature may be a *d*-*d* band related to iron, perhaps within a different local coordination environment, but offered no specific assignment.

A feature ~836 nm has been assigned previously to Fe/Fe IVCT (Rossman et al. 1982). Two Gaussian components (Supplemental Table 6b) are needed to fit this feature: 790 nm and 893 nm at room temperature. Neither is wide enough by conventional metrics (Mattson and Rossman 1987b) to be an IVCT band.

At elevated temperatures, the band system changes dramatically. The 617 nm band rapidly decreases in intensity during early heating, vanishing altogether by 300 °C. Other *d*-*d* bands at 485 and 522 nm initially broaden and increase in integral intensity, but above 500 °C, these too either vanish or become indistinct under the red shifted UV edge.

348 At 500 °C, the Fe/Ti IVCT band red shifts and broadens slightly; its integral intensity
349 decreases by 16 percent from room temperature. A broad feature at 470 nm also emerges. While
350 the red shifting of the UV absorption edge creates some uncertainty in the fitting, it is notable
351 that the appearance of the 470 nm feature in the sillimanite spectrum coincides with the
352 disappearance of the 617 nm band.

353 At 1000 °C, the shorter wavelength bands become difficult to fit accurately due to the
354 encroachment of the UV absorption edge. It is possible that additional bands exist in that region.
355 Nonetheless, all fits for sillimanite that reached convergence in its Fe/Ti IVCT band region
356 placed a broad band around 572 nm. This is significantly blue-shifted from the 612 nm
357 component at 500 °C. Assuming that only the original 592 nm room temperature IVCT
358 component band contributes significantly to its intensity, the 572 nm band at 1000 °C represents
359 only a minor change in integral absorbance (5 percent increase) from 500 °C. Given that the
360 equilibrium configuration of sillimanite at 1000 °C is clearly very distorted from that at lower
361 temperatures, it is possible that both the 470 nm and 612 nm components at 500 °C converge to
362 this band at 1000 °C. If that were the case, the decrease in integral intensity at 1000 °C from 500
363 °C would have an upper bound of 57 percent, a much larger figure.

364 The major components of the ~836 nm feature also shift drastically at 1000 °C to 726 nm and
365 856 nm. Their barycenter (12521 cm^{-1}) is similar in energy to the short wavelength component of
366 the ~836 nm feature at 500 °C (12529 cm^{-1}), indicating that between 500 and 1000 °C, additional
367 splitting of the band may occur.

368 As sillimanite is the high temperature Al_2SiO_5 polymorph, it is expected that any changes to
369 its recovery spectrum should be minor. Indeed, this is what is observed. The substantial changes

in configuration discussed previously are largely temporary, primarily only taking effect at elevated temperatures.

Andalusite (first heating). Two absorption features at room temperature are found to have half-widths consistent with IVCT bands (Supplemental Table 7a): 469 nm and 616 nm. The former has been attributed previously to Fe/Ti IVCT (Smith 1977; Taran et al. 2011). Assigning the latter is more challenging. Fe/Fe IVCT has been attributed to a feature near 14000 cm^{-1} (714 nm) (Taran et al. 2011), which is too low in energy for this band. Its parameters are more consistent with those found for the Fe/Ti IVCT bands in kyanite (Supplemental Table 5a) and sillimanite (Supplemental Table 6a).

When the sample is heated, any decrease at temperature of the 470 nm Fe/Ti IVCT band is soon obscured by the aggressively red shifting UV edge. While the UV edge feature does partially recede upon cooling, some portion of its encroachment at higher temperatures still persists in the recovery spectrum. The 616 nm IVCT feature also gains intensity with increasing temperature; this change is fully retained upon cooling.

Such changes are reasonable when a sample is being heated potentially far beyond its original formation temperature. Dehydration may also be a factor: though andalusite is nominally anhydrous, there are indications that Fe/Ti IVCT pairs and trace structural OH may be related impurities in the mineral (Taran et al. 2013). Once a sample is allowed to re-equilibrate to the imposed experimental conditions, it is expected (and observed) that recovery will improve.

This is the peer-reviewed, final accepted version for American Mineralogist, published by the Mineralogical Society of America.
The published version is subject to change. Cite as Authors (Year) Title. American Mineralogist, in press.
DOI: https://doi.org/10.2138/am-2024-9343. http://www.minsocam.org/

Andalusite (second heating). Two features at room temperature are again found (Supplemental Table 7a) to be compatible with IVCT: 475 nm and 593 nm. The sample used was highly nonuniform; the variation in band parameters between the first and second runs is likely due in part to differences between the measured spots. Similar thermal trends are observed to the first run in the second but are largely temporary; the difference between the starting and the ending room temperature spectra is negligible.

DISCUSSION

Ordinary d-d bands

Octahedral Cr^{3+} and V^{3+}. The behavior of ordinary *d-d* bands at temperature provides a useful framework within which to contextualize temperature dependent changes exhibited by IVCT bands. Single cation Cr^{3+} in octahedral coordination is a good example: it has been described elsewhere across many mineral systems (Taran et al. 1994). The absorption spectra of ruby (Supplemental Figure 8) and Cr-bearing kyanite (Supplemental Figures 9a, 9b) show typical features for $^{VI}Cr^{3+}$. The spin-allowed *d-d* bands are the most prominent. While three transitions are expected, only two ($^4A_{2g} \rightarrow {}^4T_{2g}$ and $^4A_{2g} \rightarrow {}^4T_{1g}$) are generally observed in the visible portion of optical spectra, corresponding here to the long and short wavelength bands, respectively (Taran et al. 1994). These bands in both spectra red shift and broaden markedly with heating, the usual hallmarks of a spin-allowed *d-d* band at elevated temperatures. Red shifting derives from bulk thermal expansion of the lattice: as the mean metal – oxygen distance grows, crystal field strength correspondingly decreases, leading the band center to shift towards longer wavelengths. Broadening occurs due to thermal vibrations populating additional levels in the electronic ground state.

This is the peer-reviewed, final accepted version for American Mineralogist, published by the Mineralogical Society of America.
The published version is subject to change. Cite as Authors (Year) Title. American Mineralogist, in press.
DOI: https://doi.org/10.2138/am-2024-9343. http://www.minsocam.org/

As they broaden, the spin-allowed Cr^{3+} band components simultaneously decrease in linear intensity. While some spin-allowed bands do increase in integral intensity with temperature, their corresponding transitions must be at least partially forbidden based on symmetry. Vibronic coupling relaxes symmetry selection rules as temperature increases, allowing otherwise forbidden transitions to occur between different vibrational modes of the progenitor electronic ground and excited states. Since the octahedral sites in ruby and kyanite both lack inversion centers (McClure 1962; Burnham 1963), symmetry selection rules do not pose a significant barrier to *d-d* transitions in these minerals. The effect of vibronic coupling is more substantial when a cation site is centrosymmetric, like the octahedral site in the spinel structure. The spin-allowed *d-d* bands of a V^{3+} dominant spinel (Supplemental Figure 10) broaden and grow in linear intensity; overall, their integral intensities increase at elevated temperatures.

Optical spectra dominated by crystal field transitions also often contain minor spin-forbidden features, like the ~692 nm R_1 and ~694 nm R_2 lines in the ruby spectrum (Burns 1993). Typically, just as the intensity of such bands is small, so too is their temperature dependence. In Supplemental Figures 8 and 9a,b, the spin-forbidden Cr^{3+} bands are observed to broaden but not to grow in linear intensity, becoming increasingly visually obscure with rising temperature.

Fe^{2+} and Fe^{3+}. Fe^{2+} and Fe^{3+} crystal field transitions are common in the optical spectra of iron-bearing minerals, since ferrous and ferric iron frequently co-occur in natural samples. Fe^{2+} has one spin-allowed *d-d* transition: $^5T_{2g} \rightarrow {}^5E_g$ in octahedral or $^5E \rightarrow {}^5T_2$ in tetrahedral coordination (Burns 1993). These bands are usually split into two or more components due to deviations from ideal octahedral or tetrahedral symmetry. In Fe-spinel (Figure 8) the $^{IV}Fe^{2+}$ band splits into at least four separate components placed near 1860, 2120, 2460 and 2720 nm (Rossman and Taran

2001). The longer wavelength components are cut off due to limitations on spectral range and the ability to correct for low energy NIR blackbody radiation. Discussion of changes to this spectrum at temperature focus on the prominent 1860 nm band component.

Broadening accompanies the decrease in linear intensity of the 1860 nm component. Since tetrahedral sites intrinsically lack an inversion center, spin-allowed bands of $^{IV}Fe^{2+}$ are generally more intense compared to those of Fe^{2+} in octahedral coordination, and it is not anticipated that their integral intensities should change significantly with temperature (Burns 1993). This band component blue shifts slightly with heating, which is consistent with established results of Taran and Langer (2001) who find that the barycenter of the $^5T_2$ excited state blue shifts for $^{IV}Fe^{2+}$ in spinel as well as dodecahedral Fe^{2+} in garnet. They suggest this may be due to additional splitting of the ^5E ground state at temperature. Across many minerals, they also find that trends for Fe^{2+} *d-d* bands at temperature deviate from those discussed previously for octahedral Cr^{3+}/V^{3+}, because Fe^{2+} cation sites can distort at higher temperatures to adopt significantly different geometries and symmetries from room temperature.

Unlike Fe^{2+}, Fe^{3+} has no spin-allowed *d-d* transitions: all crystal field transitions for Fe^{3+} are spin-forbidden, connecting a sextet ground state and quartet excited state. Fe^{3+} *d-d* transitions can be divided into two categories: those involving only a "spin flip" and those involving both a spin flip and an orbital change. The former tend to be more prominent; exchange interactions between Fe^{3+} cations in nearest neighbor sites significantly enhance the intensities of the spin flip bands. Exchange coupled pair (ECP) enhanced Fe^{3+} bands can represent either the single excitation of one Fe^{3+} cation in the pair or the simultaneous excitation of both cations (Ferguson and Fielding 1971, 1972).

This is the peer-reviewed, final accepted version for American Mineralogist, published by the Mineralogical Society of America.
The published version is subject to change. Cite as Authors (Year) Title. American Mineralogist, in press.
DOI: https://doi.org/10.2138/am-2024-9343. http://www.minsocam.org/

In corundum, the single excitation "spin flip" transitions $^6A_1 \rightarrow {}^4A_1, {}^4E_a$ (^4G) and $^6A_1 \rightarrow {}^4E_b$ (^4D) are assigned to the features near 455 and 377 nm, respectively (Ferguson and Fielding 1971). With heating (Figure 1), the 455 nm band broadens and red shifts slightly. Otherwise, it shows limited temperature dependence and recovers fully on cooling, which is consistent with previous findings (Taran and Langer 1998). Double excitation transitions to the $^4T_1^a + {}^4T_1^a$ and $^4T_1^a + {}^4T_2^a$ excited states have been assigned previously to absorption features near 540 and 420 nm, respectively (Ferguson and Fielding 1971), but these are typically lower intensity bands; in natural samples, their contribution to the optical spectrum is often obscured by stronger transitions (Dubinsky et al. 2020). Indeed, these bands do not contribute significantly to the spectra in Figure 1; as mentioned in the results section, it is more appropriate to assign the 558, 717, and 915 nm features to IVCT transitions.

IVCT bands. Several major conclusions may be drawn from the results above, both those specific to the aluminum oxide and aluminosilicate IVCT systems under study and those that are more general with potential implications for other IVCT systems. Minerals that grew in the earth at lower temperatures than those used in these heating experiments may undergo modest cation diffusion and reorganization of the interacting couples, such that the spectrum initially obtained on cooling the sample differs somewhat from the starting room temperature spectrum. Minerals that have gone through a high temperature heating cycle may re-equilibrate to provide a new absorption spectrum that is recovered upon a second heating and cooling cycle.

Depending on whether the Fe/Ti or Fe/Fe IVCT features dominate the spectrum of corundum, two separate configurations emerge after an initial heating run. In the first case, absorption features at short wavelengths and in the long wavelength tail increase on recovery; these changes resemble those of Al_2SiO_5 polymorphs after their first heating, especially andalusite. In the

This is the peer-reviewed, final accepted version for American Mineralogist, published by the Mineralogical Society of America.
The published version is subject to change. Cite as Authors (Year) Title. American Mineralogist, in press.
DOI: https://doi.org/10.2138/am-2024-9343. http://www.minsocam.org/

second case, the Fe/Ti bands decrease, and the Fe/Fe bands are strengthened on recovery, while the short wavelength region remains unchanged. In both cases, aggregation is likely an important factor behind the rearrangement of intensity in the spectra.

Fe/Ti IVCT. The 575 nm edge-sharing Fe/Ti band in corundum corresponds strongly to Fe/Ti IVCT bands in kyanite and sillimanite. Its band parameters at room temperature in Fe/Ti dominant corundum are almost identical to sillimanite's at 1000 °C (Supplemental Table 11), which suggests that the edge-sharing defect in corundum resembles the high temperature Fe/Ti defect in sillimanite.

At elevated temperatures, the band center shifts markedly in both Fe/Ti and Fe/Fe dominant samples; in Fe/Fe dominant corundum, the Fe/Ti component at 1000 °C may combine the edge- and face-sharing features (Supplemental Tables 12, 13). This shift pushes the energy of the 575 nm band close to the range observed for similar IVCT bands across the Al_2SiO_5 polymorphs (Supplemental Tables 14, 15), including andalusite: since its parameters are similar to those of the Fe/Ti bands in kyanite and sillimanite, the band in andalusite likely also has a similar assignment. These observations suggest that the Fe/Ti defects in corundum experience a substantial change in configuration during heating.

At higher temperatures in Fe/Ti dominant corundum, an additional broad Gaussian component is needed – on average, ~499 nm (515 nm at 500 °C, 483 nm at 1000 °C) – for a satisfactory fit. The numerical values for these and other sample fits (*ala* Supplemental Table 12a) are somewhat questionable at short wavelengths due to the breadth of absorption in this region. However, considered in reference to the other Al_2SiO_5 polymorphs (Supplemental Table 17), it is reasonable to conclude that the substance of this band appearing represents a real

change at temperature. It is possible, then, that the strong decrease of the Fe/Ti bands from room temperature to 1000 °C does include some redistribution of integrated intensity.

The new, broad short wavelength feature that emerges in corundum at elevated temperatures is understood most readily via its analogue in sillimanite: the band configuration of 500 °C sillimanite, encompassing both its Fe/Ti IVCT band and its short wavelength feature, resembles that of andalusite before heating (Supplemental Table 18). It is plausible that the 470 nm band in andalusite and the transient features in 500 °C sillimanite and high temperature corundum all involve cation clusters rather than Fe/Ti pairs. Aggregation has been found to play an important role in the thermal stability of this band in andalusite: it is more stable in dark zones than in light zones against annealing under oxidizing conditions (Taran and Koch-Müller 2011). The same authors propose that the feature has an associated "self-stabilizing effect" whereby isolated cations are encouraged to aggregate at higher temperatures.

Absorption features in ilmenite are also a helpful point of reference: in Ti2p3d resonant inelastic x-ray scattering (RIXS) spectra, two peaks associated with Fe/Ti IVCT have been observed at 280 nm and 500 nm (Agui et al. 2009). The former is common across several $MTiO_3$ species, but only $FeTiO_3$ has the latter (Agui et al. 2015). Fe K-edge 1s2pRIXS spectra and DFT calculations assign the 280 and 500 nm bands to transitions from the occupied β spin Fe t_{2g} orbital to the first Ti t_{2g} and e_g orbitals, respectively, which result from Fe 4p/Ti 3d hybridization mediated by strong O 2p/Ti 3d orbital hybridization (Hunault et al. 2017). The high temperature band in corundum corresponds reasonably well with the 500 nm feature in ilmenite, which further suggests it may be a cluster feature. Similarly, if andalusite had a Fe/Ti cluster feature at higher energies akin to the 280 nm band in ilmenite, that would be in accord with the aggressively red shifting UV absorption edge observed in heating experiments.

This is the peer-reviewed, final accepted version for American Mineralogist, published by the Mineralogical Society of America.
The published version is subject to change. Cite as Authors (Year) Title. American Mineralogist, in press.
DOI: https://doi.org/10.2138/am-2024-9343. http://www.minsocam.org/

Fe/Fe IVCT. Smith (1978) speculated that corundum's spectral features in the 833-1000 nm region may be related to Fe^{2+}/Fe^{3+} ECPs rather than Fe^{2+}/Fe^{3+} IVCT pairs. The behavior of the 907 nm (STP) Fe/Fe band in corundum during heating supports this possibility. At higher temperatures, this band splits into two components (Supplemental Table 4d). From room temperature to 1000 °C, the higher energy component blue shifts significantly; from 500 to 1000 °C, minor intensity redistribution between the two components occurs. Similar trends are also noted in Al_2SiO_5 polymorphs – primarily in sillimanite (Supplemental Table 6b) and to a lesser extent in kyanite (Supplemental Table 19). Band shifts to higher energies due to cation site deformation at elevated temperatures along with rearrangement of components and band intensity are known trends at temperature for some Fe^{2+} *d-d* bands (*ala* Figure 8).

A few observations are noteworthy here. First, parallel high temperature Fe/Fe band configurations to that of Fe/Fe dominant corundum are found in kyanite and sillimanite (Supplemental Table 20). This suggests that, as with the Fe/Ti bands, some common conclusions may be drawn for the Fe/Fe bands across these systems.

Second, Taran and Koch-Müller (2011) assigned a weak broad band near 11900 cm^{-1} (840 nm) in andalusite to the $^5T_{2g} \rightarrow {}^5E_g$ spin-allowed *d-d* transition of $^{VI}Fe^{2+}$. They attribute its energy being higher than what is typical in Mg,Fe^{2+} silicates to a difference in size between cation sites: Fe^{2+} is subject to a stronger crystal field when substituting for Al^{3+} rather than Mg^{2+}. Bands components with centers or barycenters comparable to this in energy are observed in sillimanite (Supplemental Table 6b) and kyanite (Supplemental Table 19); the higher energy Fe/Fe component in corundum (Supplemental Table 21) also has a similar band center.

Third, while the room temperature spectra for Fe/Fe and Fe/Ti corundum differ significantly, the Fe/Fe band configuration of Fe/Fe corundum at 1000 °C strongly resembles that of Fe/Ti

This is the peer-reviewed, final accepted version for American Mineralogist, published by the Mineralogical Society of America.
The published version is subject to change. Cite as Authors (Year) Title. American Mineralogist, in press.
DOI: https://doi.org/10.2138/am-2024-9343. http://www.minsocam.org/

corundum (Supplemental Table 21). This is consistent with the fact that the parameters of the Fe/Ti bands in Fe/Fe corundum also converge at higher temperatures to similar values as those of Fe/Ti corundum (Supplemental Tables 12, 13) and suggests that the high temperature equilibrated configuration of Fe/Ti corundum may be significantly distorted relative to Fe/Fe corundum.

Fourth, the split components of the 907 nm band shift significantly with heating; the barycenter of the band (assuming octahedral splitting) does not, experiencing only a slight red shift (209 cm^{-1}) from room temperature to 1000 °C. Minor red shifting and reduced integral intensity align with previously observed thermal trends for IVCT bands (Taran and Langer 1998); they also align with previously observed thermal trends for ECP-enhanced Fe^{2+} *d-d* bands (Taran et al. 1996). The Fe/Fe band in corundum decreases more markedly in intensity than any Fe/Fe ECP bands reported on by the previous authors. However, the total integral intensity for both components of the 907 nm (STP) band in Fe/Fe dominant corundum changes little between 500 and 1000 °C (Supplemental Table 4d), which matches observed thermal trends in tourmaline: the integral intensities of Fe/Fe ECP bands decrease "approximately down to intensities of ordinary dd-bands" until ~700 K, above which they "remain almost constant" (Taran et al. 1996).

These observations suggest that bands assigned to Fe/Fe IVCT in corundum have some mixed Fe^{2+} *d-d* character; they may represent more metal-centered electron transfer, which would be consistent with similar bands in synthetic organometallic molecular species (Turlington et al. 2016; Livshits et al. 2019). More detailed theoretical work would likely be required to fully characterize this feature.

This is the peer-reviewed, final accepted version for American Mineralogist, published by the Mineralogical Society of America.
The published version is subject to change. Cite as Authors (Year) Title. American Mineralogist, in press.
DOI: https://doi.org/10.2138/am-2024-9343. http://www.minsocam.org/

Finally, like the short wavelength feature in Fe/Ti corundum, the 907 nm feature in Fe/Fe corundum may correspond to a cluster, not a pair. An Fe^{2+}–Ti^{4+}–Fe^{3+} cluster is plausible, as it increases at the expense of the Fe/Ti IVCT feature in samples with relatively high iron content.

A common observation. Across all samples examined, the integral intensity of IVCT bands significantly decreases from room temperature to 1000 °C. In some cases, the decreases in intensities of the IVCT features by 1000 °C are essentially complete.

IMPLICATIONS

Assessing how general the loss of intensity experienced by IVCT bands is at elevated temperatures would require exploration across more varied mineral systems, but it may represent an important criterion for establishing the origin of features in optical spectra. Of greater significance may be how these features behave in mantle minerals with higher concentrations of IVCT: the thermal behavior of such phases potentially has bearing on calculations of radiative conductivity in the Earth. Some indications exist that many of the IVCT bands examined here represent clusters rather than isolated pairs; the complex changes these dilute systems show at temperature suggest that the investigation of higher concentration IVCT species will be an interesting avenue of inquiry.

ACKNOWLEDGMENTS AND FUNDING

Samples used in the study were obtained from Ed Grew, Paul Brian Moore, The American Museum of Natural History, Art Boettcher, William F. Larson, Ed Swobota, Richard Hughes, and John Emmett who is also thanked for several helpful discussions regarding corundum. This research was supported by grant EAR-2148727 from the National Science Foundation and by the White Rose Foundation.

REFERENCES CITED

Agui, A., Uozumi, T., Mizumaki, M., and Käämbre, T. (2009). Intermetallic charge transfer in $FeTiO_3$ probed by resonant inelastic soft x-ray scattering. Physical Review B, 79(9), 092402. https://doi.org/10.1103/PhysRevB.79.092402

Agui, A., Mizumaki, M., and Uozumi, T. (2015). Intermetallic charge transfer in $MTiO_3$ (M=Mn, Fe, Co, and Ni) by Ti 2p edge resonant inelastic X-ray scattering. Journal of Electron Spectroscopy and Related Phenomena, 205, 106–110. https://doi.org/10.1016/j.elspec.2015.08.017

Allen, G. C., & Hush, N. S. (1967). Intervalence-transfer absorption. I. Qualitative evidence for intervalence-transfer absorption in inorganic systems in solution and in the solid state. *Progress in Inorganic Chemistry*, *8*, 357–444. https://doi.org/10.1002/9780470166093.ch6

Amthauer, G., and Rossman, G.R. (1984). Mixed valence of iron in minerals with cation clusters. Physics and Chemistry of Minerals, 11(1), 37–51. https://doi.org/10.1007/BF00309374

Blasse, G. (1991). Optical electron transfer between metal ions and its consequences. Complex Chemistry, 153–187.

Bristow, J.K., Tiana, D., Parker, S.C., and Walsh, A. (2014). Defect chemistry of Ti and Fe impurities and aggregates in Al2O3. Journal of Materials Chemistry A, 2(17), 6198–6208. https://doi.org/10.1039/C3TA15322C

Burnham, C.W. (1963). Refinement of the crystal structure of kyanite. Zeitschrift Für Kristallographie, 118(5–6), 337–360. https://doi.org/10.1524/zkri.1963.118.5-6.337

Burns, R.G. (1993). Mineralogical Applications of Crystal Field Theory (Second edition). Massachusetts Institute of Technology, Cambridge, Massachusetts: Cambridge University Press

Dubinsky, E.V., Stone-Sundberg, J., and Emmett, J.L. (2020). A quantitative description of the causes of color in corundum. Gems & Gemology, 56(1), 1–27.

Emmett, J. L., & Douthit, T. R. (1993). Heat Treating the Sapphires of Rock Creek, Montana. *Gems & Gemology*, *29*(4), 250–272.

Ferguson, J., and Fielding, P.E. (1971). The origins of the colours of yellow, green and blue sapphires. Chemical Physics Letters, 10(3), 262–265. https://doi.org/10.1016/0009-2614(71)80282-8

Ferguson, J., and Fielding, P. (1972). The origins of the colours of natural yellow, blue, and green sapphires. Australian Journal of Chemistry, 25(7), 1371–1385.

Fritsch, E., and Rossman, G.R. (1988). An update on color in gems. Part 2: Colors involving multiple atoms and color centers. Gems & Gemology, 24(1), 3–15.

Geiger, C.A., and Taran, M.N. (2023). Single-crystal UV/Vis absorption spectroscopy of aluminosilicate garnet: Part III. $\{Fe^{2+}\} + [Fe^{3+}] \rightarrow \{Fe^{3+}\} + [Fe^{2+}]$ intervalence charge transfer. American Mineralogist, 108(6), 1171–1181. https://doi.org/10.2138/am-2022-8756

Grose, C.J., and Afonso, J.C. (2019). New constraints on the thermal conductivity of the upper mantle from numerical models of radiation transport. Geochemistry, Geophysics, Geosystems, 20(5), 2378-2394.

Hammarström, L. (2015). Accumulative Charge Separation for Solar Fuels Production: Coupling Light-Induced Single Electron Transfer to Multielectron Catalysis. Accounts of Chemical Research, 48, 840–850.

Hofmeister, A.M. (2005). Dependence of diffusive radiative transfer on grain-size, temperature, and Fe-content: Implications for mantle processes. Journal of Geodynamics, 40(1), 51–72.

Hunault, M.O.J.Y., Khan, W., Minár, J., Kroll, T., Sokaras, D., Zimmermann, P., Delgado-Jaime, M.U., and de Groot, F.M.F. (2017). Local vs Nonlocal States in $FeTiO_3$ Probed with 1s2pRIXS: Implications for Photochemistry. Inorganic Chemistry, 56(18), 10882–10892. https://doi.org/10.1021/acs.inorgchem.7b00938

Hush, N. S. (1967). Intervalence-transfer absorption. Part 2. Theoretical considerations and spectroscopic data. Progress in Inorganic Chemistry, 8, 391–444. https://doi.org/10.1002/9780470166093.ch7

Hush, N. S. (1968). Homogeneous and Heterogeneous Optical and Thermal Electron Transfer. *Electrochimica Acta*, *13*, 1005–1023.

Keppler, H., and Smyth, J.R. (2005). Optical and near infrared spectra of ringwoodite to 21.5 GPa: Implications for radiative heat transport in the mantle. American Mineralogist, 90(7), 1209–1212. https://doi.org/10.2138/am.2005.1908

Keppler, H., Dubrovinsky, L.S., Narygina, O., and Kantor, I. (2008). Optical Absorption and Radiative Thermal Conductivity of Silicate Perovskite to 125 Gigapascals. Science, 322 (December), 1529–1532.

Lin, J., Speziale, S., Mao, Z., and Marquardt, H. (2013). Effects of the Electronic Spin Transitions of Iron in Lower Mantle Minerals: Implications for Deep Mantle Geophysics and Geochemistry. Reviews of Geophysics, (2012), 244–275. https://doi.org/10.1002/rog.20010.1.INTRODUCTION

Livshits, M.Y., Turlington, M.D., Trindle, C.O., Wang, L., Altun, Z., Wagenknecht, P.S., and Rack, J.J. (2019). Picosecond to Nanosecond Manipulation of Excited-State Lifetimes in

659 Complexes with an FeII to TiIV Metal-to-Metal Charge Transfer: The Role of Ferrocene
660 Centered Excited States. Inorganic Chemistry, 58(22), 15320–15329.
661 https://doi.org/10.1021/acs.inorgchem.9b02316

662 Mattson, S.M., and Rossman, G.R. (1987a). Fe^{2+} Fe^{3+} Interactions in Tourmaline. Physics and
663 Chemistry of Minerals, 14(1987), 163–171.

664 Mattson, S.M., and Rossman, G.R. (1987b). Identifying characteristics of charge transfer
665 transitions in minerals. Physics and Chemistry of Minerals, 14(1), 94–99.
666 https://doi.org/10.1007/BF00311152

667 Mattson, S.M., and Rossman, G.R. (1988). Fe^{2+}-Ti^{4+} charge transfer in stoichiometric Fe^{2+},Ti^{4+}-
668 minerals. Physics and Chemistry of Minerals, 16(1), 78–82.

669 McClure, D.S. (1962). Optical Spectra of Transition Metal Ions in Corundum. The Journal of
670 Chemical Physics, 36(10), 2757–2779. https://doi.org/10.1063/1.1732364

671 Moon, A.R., and Phillips, M.R. (1994). Defect clustering and color in Fe, Ti: α-Al_2O_3. Journal of
672 the American Ceramic Society, 77, 356–367.

673 Parkin, K.M., Loeffler, B.M., and Burns, R.G. (1977). Mössbauer spectra of kyanite,
674 aquamarine, and cordierite showing intervalence charge transfer. Physics and Chemistry of
675 Minerals, 1, 301–311.

676 Platonov, A.N., Tarashchan, A.N., Langer, K., Andrut, M., Partzsch, G., and Matsyuk, S.S.
677 (1998). Electronic absorption and luminescence spectroscopic studies of kyanite single
678 crystals: Differentiation between excitation of FeTi charge transfer and Cr^{3+} dd transitions.
679 Physics and Chemistry of Minerals, 25, 203–212.

680 Rossman, G.R., Grew, E.S., and Dollase, W.A. (1982). The colors of sillimanite. American
681 Mineralogist, 67(7–8), 749–761.

Rossman, G.R., and Taran, Michail N. (2001). Spectroscopic standards for four- and fivefold-coordinated Fe2+ in oxygen-based minerals. American Mineralogist, 86(7–8), 896–903. https://doi.org/10.2138/am-2001-0713

Rossman, G.R. (2024). Mineral Spectroscopy Server [dataset]. https://doi.org/10.7907/jywr-qq57

Rüscher, C.H. (2012). Temperature-dependent absorption of biotite: small-polaron hopping and other fundamental electronic excitations. Eur. J. Mineral., 24(February), 817–822. https://doi.org/10.1127/0935-1221/2012/0024-2200

Sherman, D.M. (1987a). Molecular Orbital (SCF-Xα-SW) Theory of Metal-Metal Charge Transfer Processes in Minerals: I. Application to $Fe^{2+} \rightarrow Fe^{3+}$ Charge Transfer and "Electron Delocalization" in Mixed-Valence Iron Oxides and Silicates. Journal of Physics and Chemistry of Solids, 14, 355–363.

Sherman, D.M. (1987b). Molecular Orbital (SCF-Xα-SW) Theory of Metal-Metal Charge Transfer Processes in Minerals: II. Application to $Fe^{2+} \rightarrow Ti^{4+}$ Charge Transfer Transitions in Oxides and Silicates. Physics and Chemistry of Minerals, 14, 364–367.

Smith G., Strens R.G.J. (1976) Intervalence-transfer absorption in some silicate, oxide and phosphate minerals. In Physical Chemistry of Rocks & Minerals, Strens RGJ, New York, J Wiley and Sons, p 584-612.

Smith, G. (1977). Low-Temperature Optical Studies of Metal-Metal Charge-Transfer Transitions in Various Minerals. Canadian Mineralogist, 15, 500–507. Retrieved from http://rruff.info/doclib/cm/vol15/CM15_500.pdf

Smith, G. (1978). Evidence for absorption by exchange-coupled Fe^{2+}-Fe^{3+} pairs in the near infra-red spectra of minerals. Physics and Chemistry of Minerals, 3(4), 375–383. https://doi.org/10.1007/BF00311848

705 Taran, M.N., Langer, K., Platonov, A.N., and Indutny, V.V. (1994). Optical-Absorption
706 Investigation of Cr^{3+} Ion-Bearing Minerals in the Temperature-Range 77-797 K. Physics and
707 Chemistry of Minerals, 21(6), 360–372. https://doi.org/10.1007/BF00203294
708 Taran, M.N., Langer, K., and Platonov, A.N. (1996). Pressure- and temperature-effects on
709 exchange-coupled-pair bands in electronic spectra of some oxygen-based iron-bearing
710 minerals. Physics and Chemistry of Minerals, 23(4–5), 230–236.
711 https://doi.org/10.1007/BF00207754
712 Taran, M.N., and Langer, K. (1998). Temperature and pressure dependence of intervalence
713 charge transfer bands in spectra of some Fe- and Fe,Ti-bearing oxygen-based minerals. N. Jb.
714 Miner. Abh., 172(2/3), 325–246.
715 Taran, M.N., and Langer, K. (2001). Electronic absorption spectra of Fe^{2+} ions in oxygen-based
716 rock-forming minerals at temperatures between 297 and 600 K. Physics and Chemistry of
717 Minerals, 28, 199–210.
718 Taran, M.N., Koch-Müller, M., and Langer, K. (2005). Electronic absorption spectroscopy of
719 natural (Fe^{2+}, Fe^{3+})-bearing spinels of spinel s.s.-hercynite and gahnite-hercynite solid
720 solutions at different temperatures and high-pressures. Physics and Chemistry of Minerals,
721 32(3), 175–188. https://doi.org/10.1007/s00269-005-0461-z
722 Taran, M.N., Dyar, M.D., and Matsyuk, S.S. (2007). Optical absorption study of natural garnets
723 of almandine-skiagite composition showing intervalence Fe^{2+}+ Fe^{3+}→ Fe^{3+}+ Fe^{2+}charge-
724 transfer transition. American Mineralogist, 92(5–6), 753–760.
725 https://doi.org/10.2138/am.2007.2163

726 Taran, M.N., and Koch-Müller, M. (2011). Optical absorption of electronic Fe-Ti charge-transfer
727 transition in natural andalusite: The thermal stability of the charge-transfer band. Physics and
728 Chemistry of Minerals, 38(3), 215–222. https://doi.org/10.1007/s00269-010-0397-9
729 Taran, M.N., and Koch-Müller, M. (2013). FTIR spectroscopic study of natural andalusite
730 showing electronic Fe – Ti charge-transfer processes : zoning and thermal evolution of OH-
731 vibration bands. Physics and Chemistry of Minerals, 40, 63–71.
732 https://doi.org/10.1007/s00269-012-0547-3
733 Taran, M.N. (2019). Electronic intervalence $Fe^{2+} + Ti^{4+} \rightarrow Fe^{3+} + Ti^{3+}$ charge-transfer transition
734 in ilmenite. Physics and Chemistry of Minerals, 46, 839–843.
735 Turlington, M.D., Pienkos, J.A., Carlton, E.S., Wroblewski, K.N., Myers, A.R., Trindle, C.O.,
736 Altun, Z., Rack, J.J., and Wagenknecht, P.S. (2016). Complexes with Tunable Intramolecular
737 Ferrocene to TiIV Electronic Transitions: Models for Solid State FeII to TiIV Charge
738 Transfer. Inorganic Chemistry, 55(5), 2200–2211.
739 https://doi.org/10.1021/acs.inorgchem.5b02587
740 Ullrich, K., Langer, K., and Becker, K.D. (2002). Temperature dependence of the polarized
741 electronic absorption spectra of olivines. Part I – fayalite. Physics and Chemistry of Minerals,
742 29, 409–419. https://doi.org/10.1007/s00269-002-0248-4
743 Ullrich, K., Ott, O., Langer, K., and Becker, K.D. (2004). Temperature dependence of the
744 polarized electronic absorption spectra of olivines. Part II—Cobalt-containing olivines.
745 Physics and Chemistry of Minerals, 31, 247–260.

This is the peer-reviewed, final accepted version for American Mineralogist, published by the Mineralogical Society of America.
The published version is subject to change. Cite as Authors (Year) Title. American Mineralogist, in press.
DOI: https://doi.org/10.2138/am-2024-9343. http://www.minsocam.org/

Figure 1.

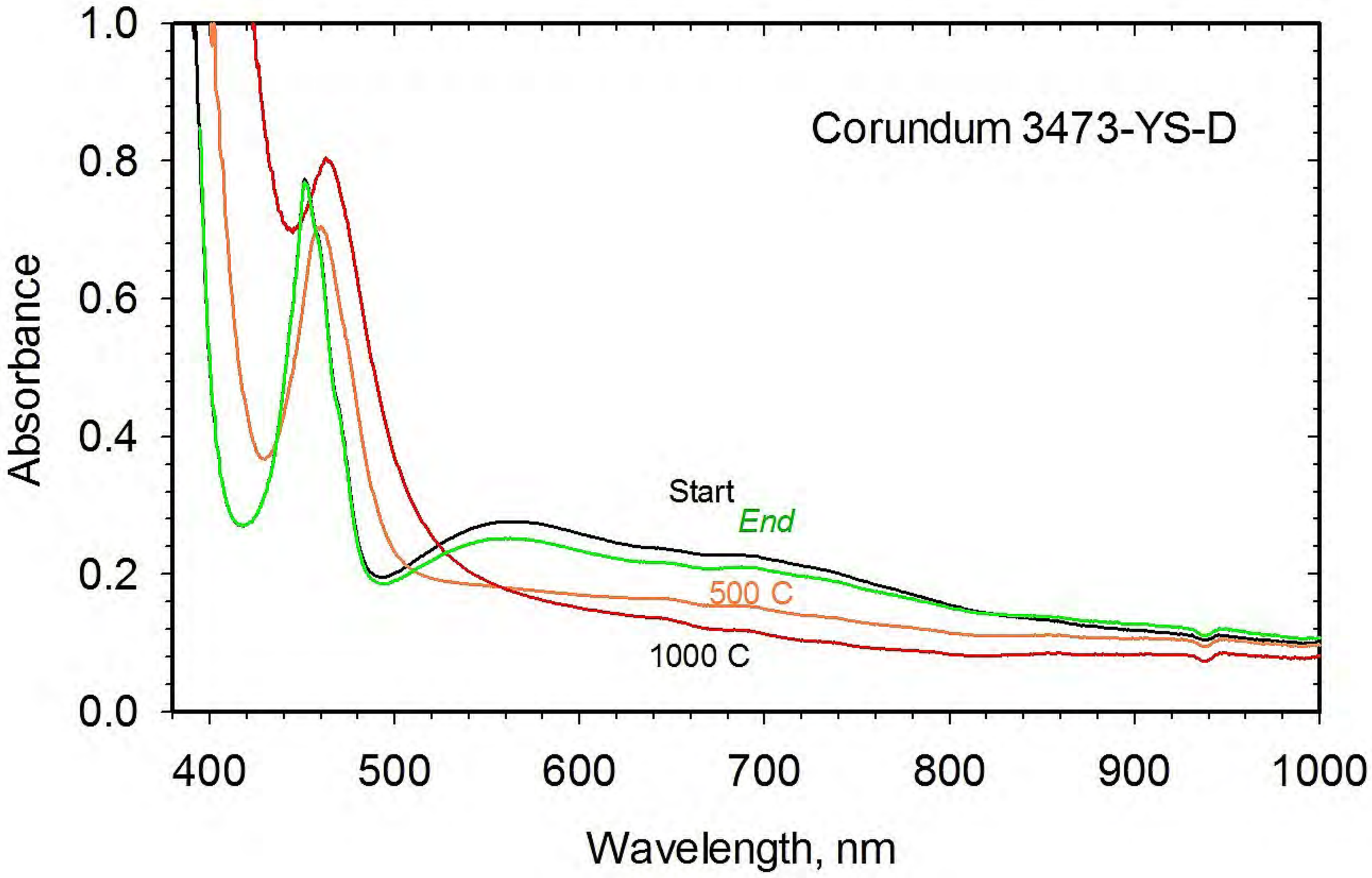

This is the peer-reviewed, final accepted version for American Mineralogist, published by the Mineralogical Society of America.
The published version is subject to change. Cite as Authors (Year) Title. American Mineralogist, in press.
DOI: https://doi.org/10.2138/am-2024-9343. http://www.minsocam.org/

Figure 2.

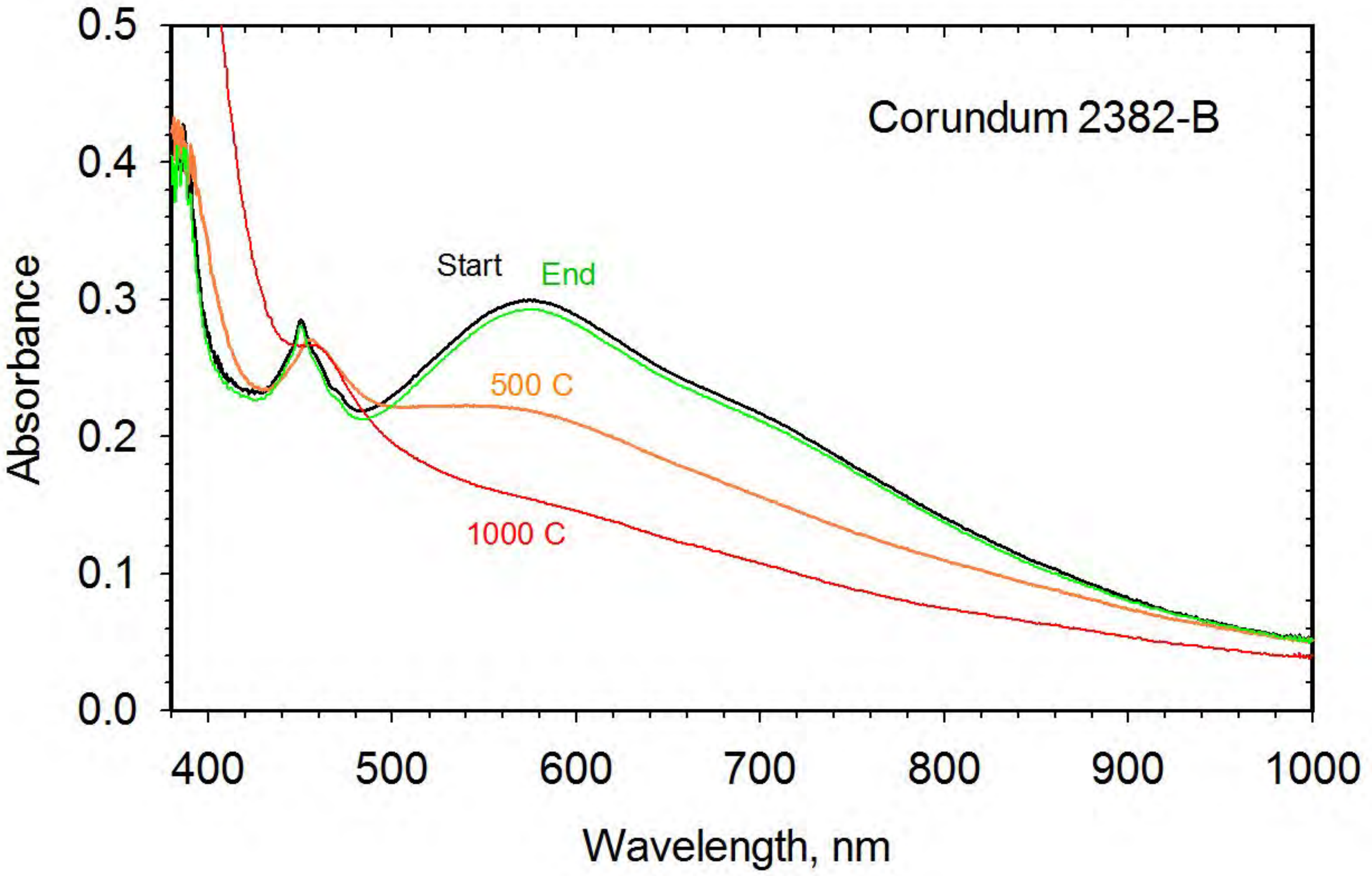

This is the peer-reviewed, final accepted version for American Mineralogist, published by the Mineralogical Society of America.
The published version is subject to change. Cite as Authors (Year) Title. American Mineralogist, in press.
DOI: https://doi.org/10.2138/am-2024-9343. http://www.minsocam.org/

Figure 3.

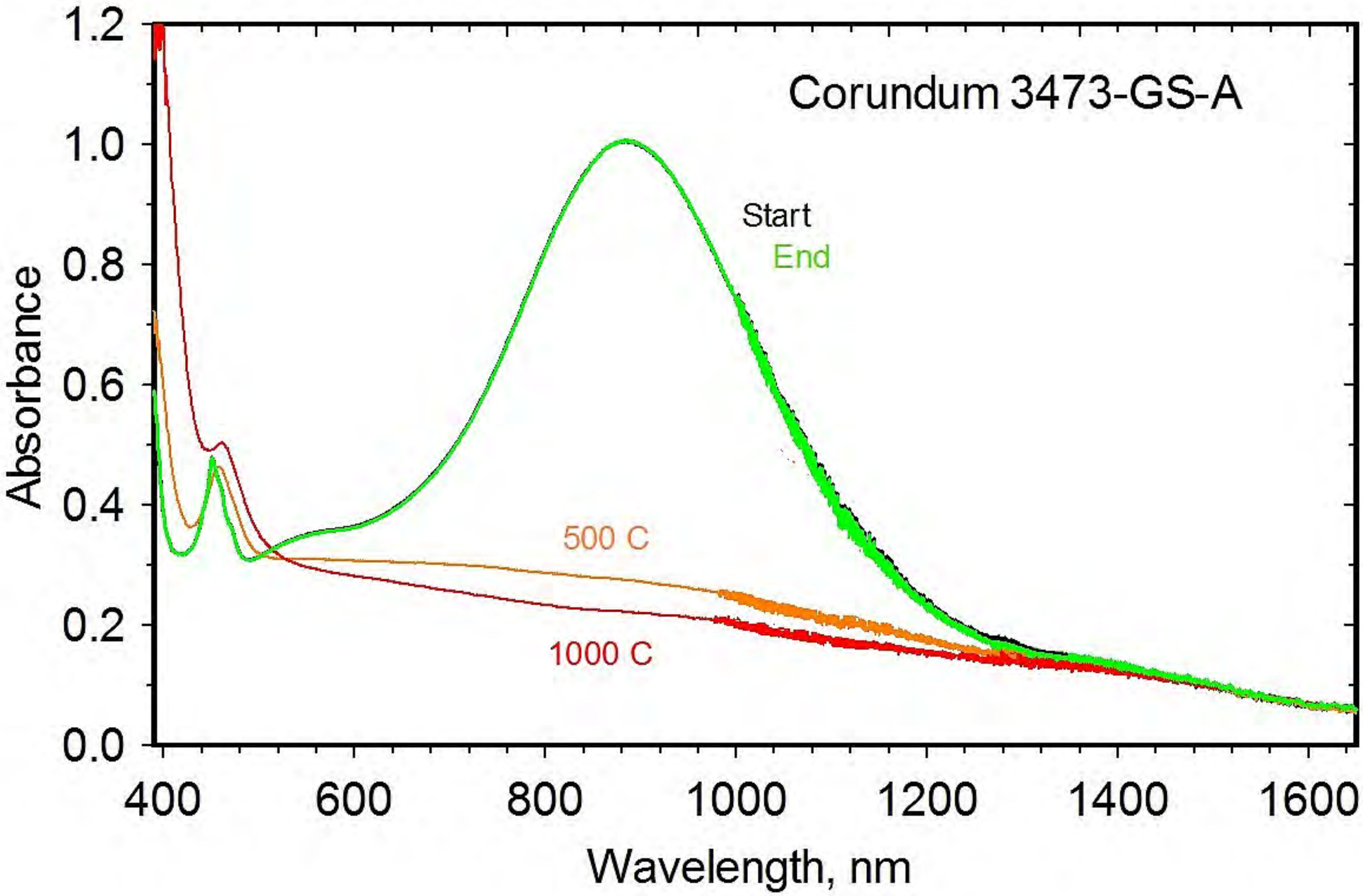

This is the peer-reviewed, final accepted version for American Mineralogist, published by the Mineralogical Society of America.
The published version is subject to change. Cite as Authors (Year) Title. American Mineralogist, in press.
DOI: https://doi.org/10.2138/am-2024-9343. http://www.minsocam.org/

Figure 4.

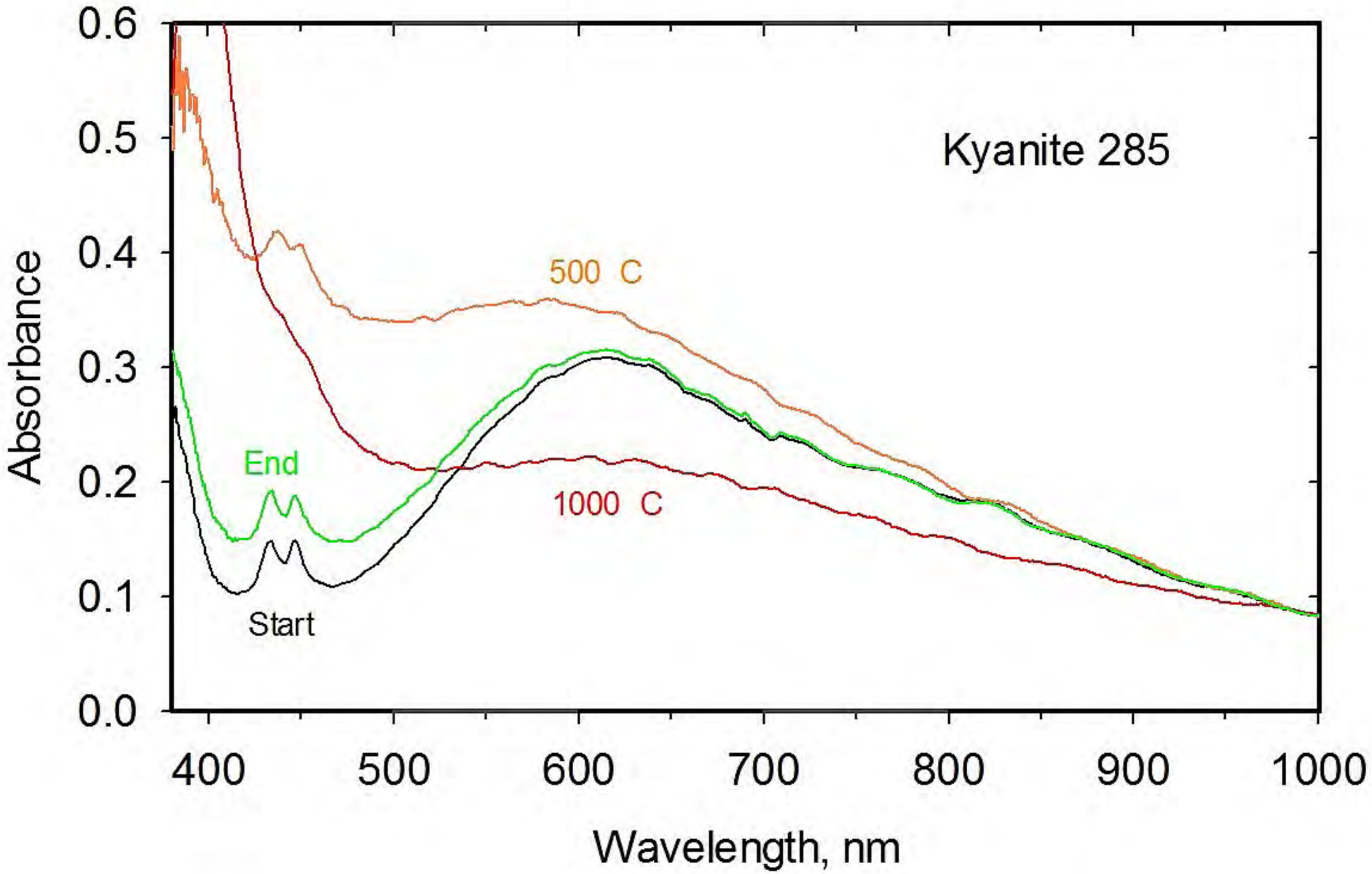

This is the peer-reviewed, final accepted version for American Mineralogist, published by the Mineralogical Society of America.
The published version is subject to change. Cite as Authors (Year) Title. American Mineralogist, in press.
DOI: https://doi.org/10.2138/am-2024-9343. http://www.minsocam.org/

Figure 5.

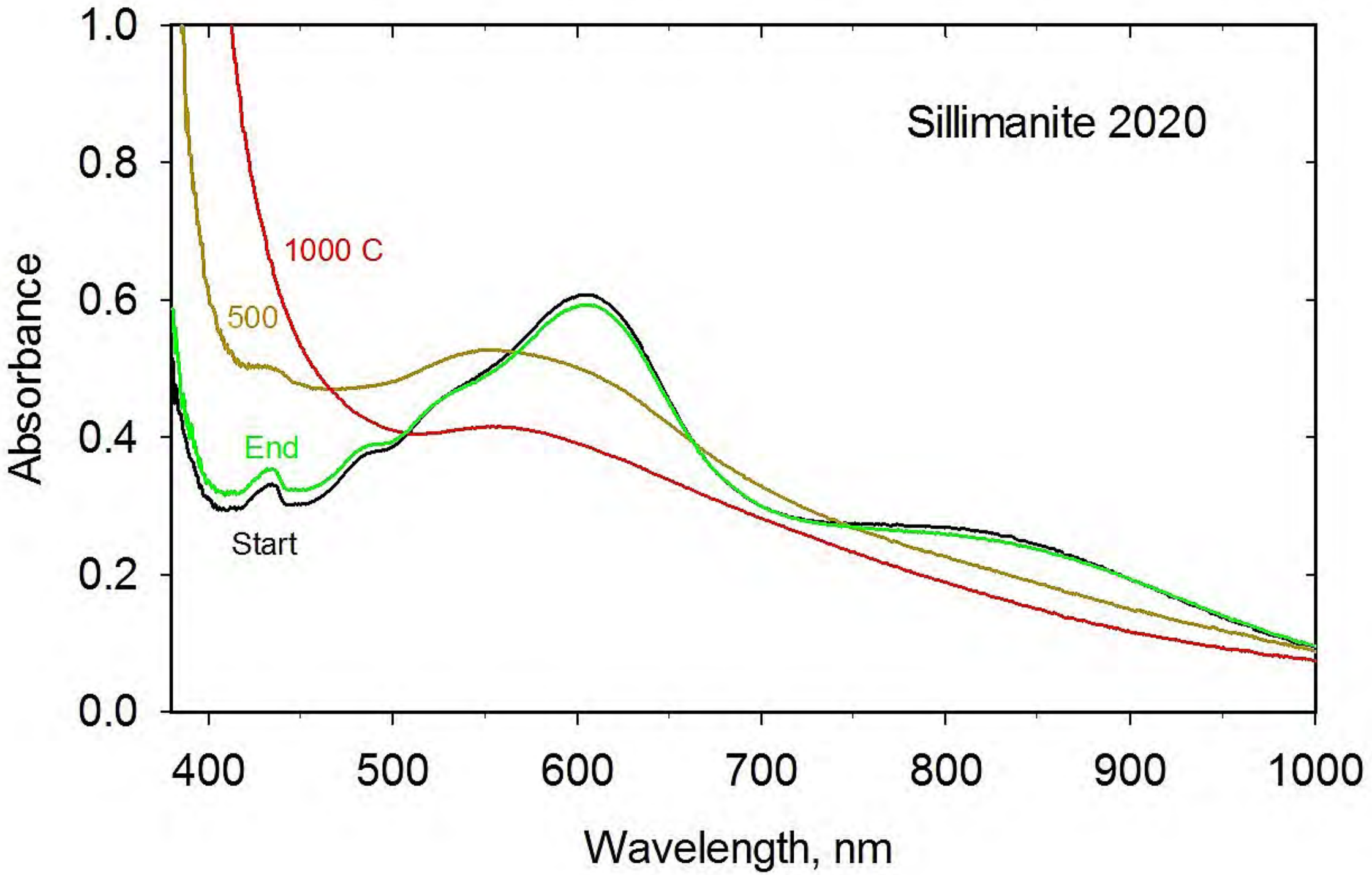

This is the peer-reviewed, final accepted version for American Mineralogist, published by the Mineralogical Society of America.
The published version is subject to change. Cite as Authors (Year) Title. American Mineralogist, in press.
DOI: https://doi.org/10.2138/am-2024-9343. http://www.minsocam.org/

Figure 6.

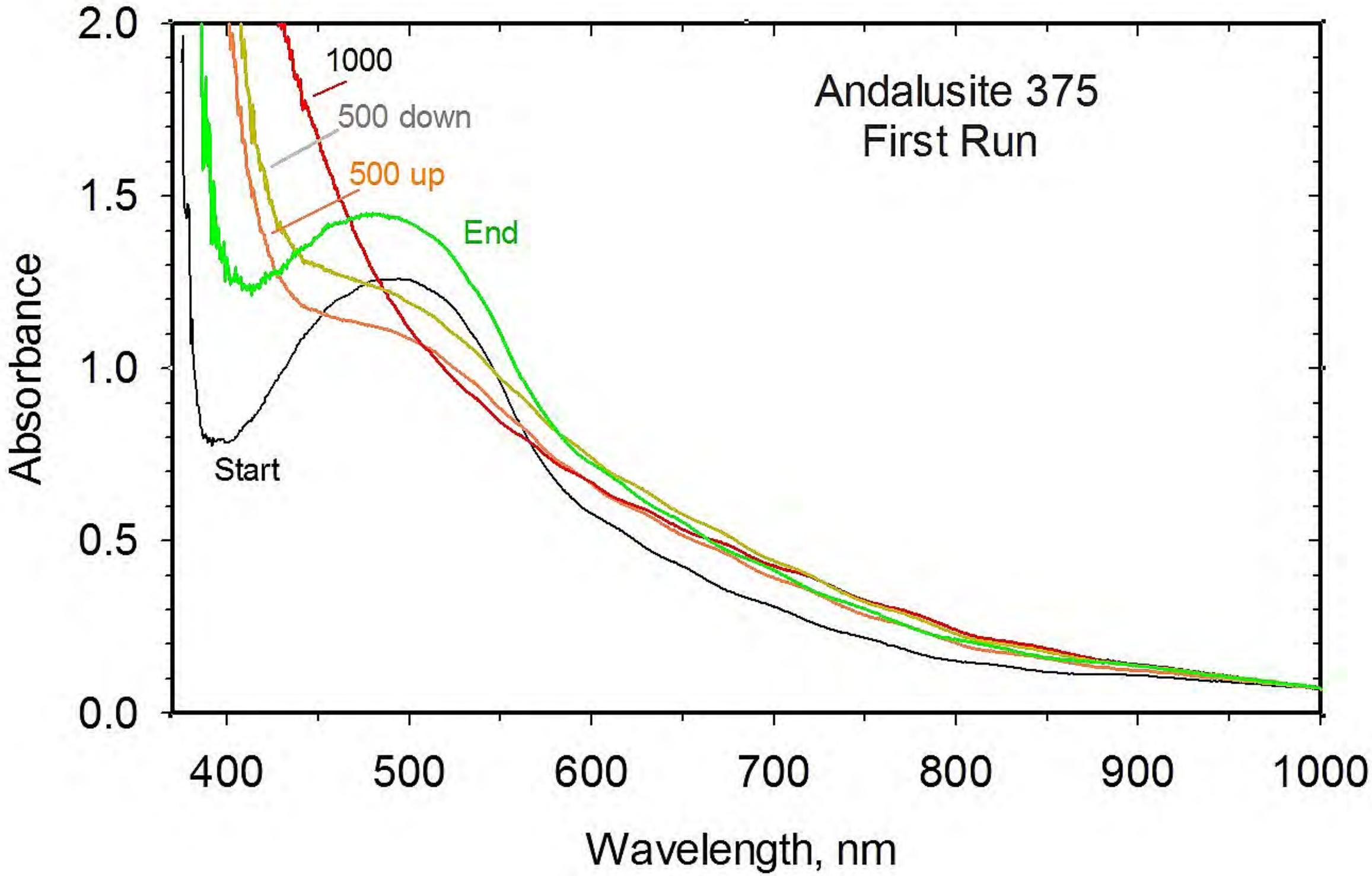

This is the peer-reviewed, final accepted version for American Mineralogist, published by the Mineralogical Society of America.
The published version is subject to change. Cite as Authors (Year) Title. American Mineralogist, in press.
DOI: https://doi.org/10.2138/am-2024-9343. http://www.minsocam.org/

Figure 7.

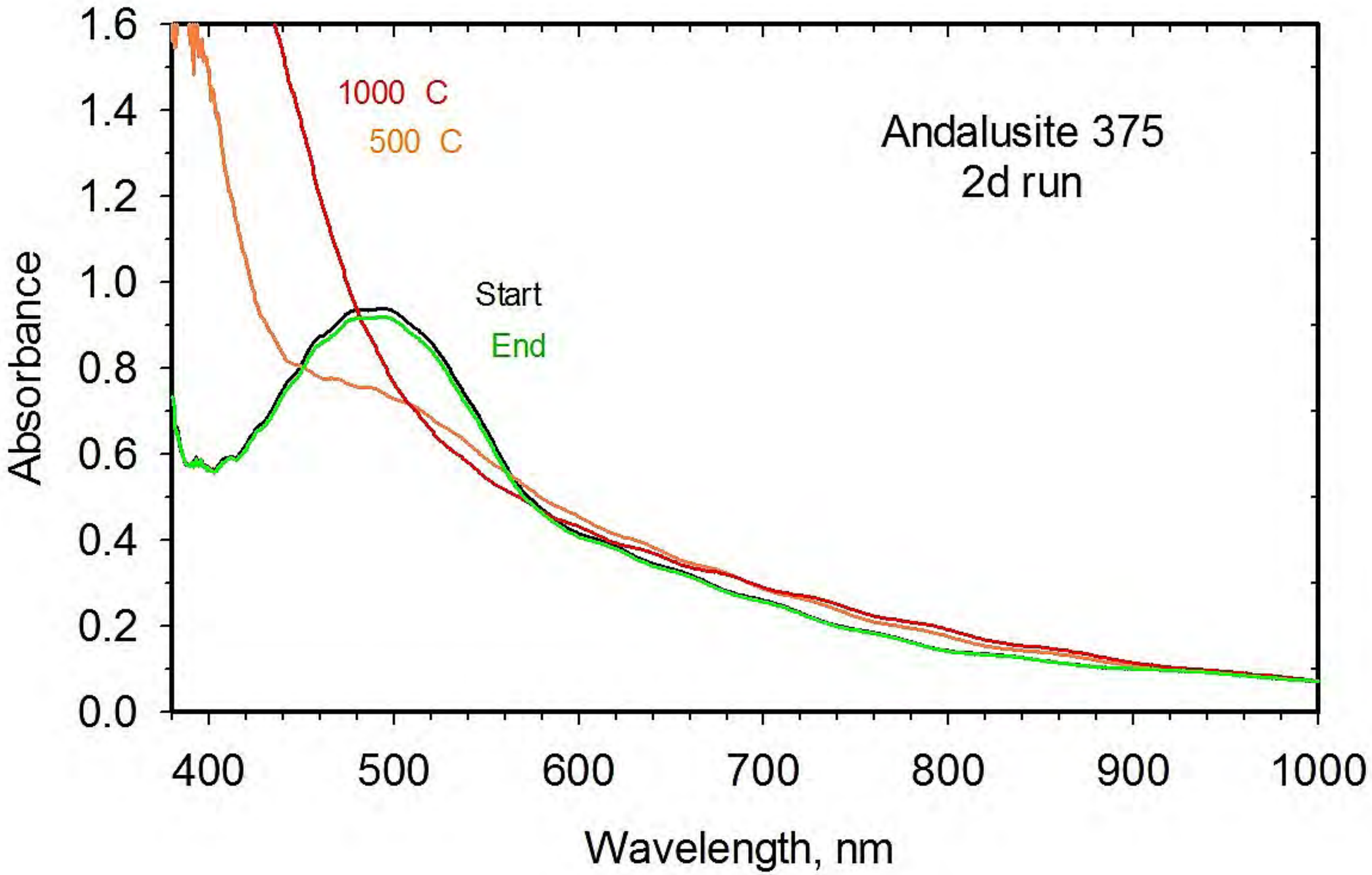

This is the peer-reviewed, final accepted version for American Mineralogist, published by the Mineralogical Society of America.
The published version is subject to change. Cite as Authors (Year) Title. American Mineralogist, in press.
DOI: https://doi.org/10.2138/am-2024-9343. http://www.minsocam.org/

Figure 8.